SUPPLEMENTARY MATERIALS

INTRODUCTION

Precise evidence of the effectiveness of targeting YAP1/TAZ–TEAD has been limited to the use of verteporfin (Liu-Chittenden et al., 2012) and peptide inhibitors (Jiao et al., 2014; Zhang et al., 2014). One problem with this approach is that verteporfin has YAP1/TAZ–TEAD–independent effects (AlAmri et al., 2018; Scott and Goa, 2000), and drugs and soluble peptide inhibitors do not provide cellular and tissue level information. In contrast, studies of the role of YAP1/TAZ in cancer involve the knockout of these proteins, affecting TEAD-dependent events and other transcriptional and signaling components that interact with YAP1 and TAZ (McNeill and Woodgett, 2010; Piccolo et al., 2014). This complicates the precise understanding of TEAD functions and masks the potential differences between the absence and blockage of YAP1/TAZ proteins. An additional tool to study TEAD specificity is rescue experiments with the YAP1 S94/F95 mutant that does not bind to TEAD (Li et al., 2010), although YAP1 and TAZ have to be knocked down or knocked out for these assays, and the rescue leads to YAP1 overexpression.

DISCUSSION

TEAD inhibition in basal cell carcinoma (BCC) leads to differentiation and elimination of tumor cells, making TEAD inhibitors (TEADis) candidates for differentiation therapy (de Thé, 2018). Nevertheless, our data indicate that cells that evade the activation of differentiation pathways could be less sensitive to TEAD blockage. Furthermore, potential tumor-promoting and immune-evasion signals mediated by cytoplasmic interactions of YAP1 and TAZ could pose a challenge on targeting this pathway because blocking TEAD would not be able to prevent non-nuclear effects of YAP1/TAZ. Inhibitors that target cytoplasmic and nuclear functions of YAP1 and TAZ could prove to be more effective for cancer treatment. In this regard, we found that the transcriptional networks activated by YAP1/TAZ knockdown present high similarity with those activated by cAMP and protein kinase A signaling. Indeed, cAMP and protein kinase A blockage can lead to BCC formation by inducing the cell-autonomous activation of GLI and YAP1 (Iglesias-Bartolome et al., 2015). Activation of protein kinase A on the other hand can lead to blockage of YAP1 function (Iglesias-Bartolome et al., 2015; Kim et al., 2013; Yu et al., 2013). Forskolin, which results in increased intracellular cAMP levels and protein kinase A activation, has been shown to reduce BCC tumor formation in mouse models (Makinodan and Marneros, 2012), highlighting the potential of this pathway for YAP1/TAZ inhibition and BCC treatment.

SUPPLEMENTARY MATERIALS AND METHODS

Cell culture, transfections, and adenoviral transductions

Cells were cultured at 37 °C in the presence of 5% carbon dioxide. BCC tumor cells were isolated from the tail skin of keratin 14 (K14)-*SmoM2* mice five weeks after tamoxifen induction. The skin was disinfected with 10% iodine in PBS and incubated with 2 U/ml of dispase (STEMCELL Technologies, Vancouver, Canada) overnight at 4 °C. The next day, the epidermis was scraped with forceps and digested with trypsin 0.05% + EDTA solution (Sigma-Aldrich, St. Louis, MO) at 37 °C for 4 minutes. Cells were filtered using a 100-µm cell strainer, pelleted at 400 g, and plated in collagen I–coated dishes (0.3 mg/ml collagen I, Corning, Corning, NY, in 1% acetic acid). BCC cells were cultured using EpiLife medium with 60 µM calcium (Gibco, Waltham, MA, MEPI500CA), supplemented with defined growth supplement (EDGS, Gibco, S0125), mouse EGF (10 ng/ml, R&D Systems, Minneapolis, MN, 2028EG200), and Y-27632 compound (10 µM, Tocris Bioscience, Bristol, United Kingdom, 12-541-0). N/TERT2G human keratinocytes were cultured as described before (Yuan et al., 2020). For small interfering RNA (siRNA) experiments, cells were transfected with the corresponding siRNAs 1 day after plating and were treated/harvested 48 hours after transfection. siRNAs were siGENOME SMARTpool from Dharmacon/Horizon, small interfering RNAs targeting YAP1 (M-046247-01-0010), small interfering RNAs targeting TAZ (Wwtr1, M-041057-01-0010), KLF4 by pooled small interfering RNAs (M-040001-02-0010), small interfering RNAs targeting SNAI2 (M-042291-00-0005), and nontargeting control siRNA (D-001206-13). siRNA was transfected at a concentration of 8 pmol cm^{-2} using Lipofectamine RNAiMAX (Invitrogen, Waltham, MA) according to the manufacturer's instructions. For adenoviral transduction, cells were incubated with a multiplicity of infection of 25. Adenoviruses were produced, purified, and titered by Vector Biolabs (Malvern, PA) in an adenoviral-type 5 (dE1/E3) backbone with a CMV promoter: Ad-CMV-TEADi (custom); Ad-CMV-KLF4, catalog number 1787; and Ad-CMV-GFP, catalog number 1060. For proliferation analysis, cells were plated in 96-well plates and transduced with indicated constructs, and proliferation was measured using CellTiter-Glo Luminescent Cell Viability Assay (Promega, Madison, WI). To assess colony-forming efficiency, an equal number of keratinocytes from corresponding mice were infected with adenoviruses expressing GFP, adenoviruses expressing a GFP-tagged TEAD inhibitor, or adenoviruses expressing KLF4 and were plated in triplicate in six-well plates and grown for 5–7 days. Plates were fixed using 4% formaldehyde for 15 minutes and stained with crystal blue (0.5%, Sigma-Aldrich).

Gene expression analysis

RNA was isolated using TRIzol Reagent (Invitrogen) according to the manufacturer's instructions. Cells were lysed using Precellys lysing kit (Bertin Instruments, Montigny-le-Bretonneux, France), and mRNA integrity was validated with Agilent TapeStation system. Three independent samples were sequenced for each condition. mRNA expression profiling was performed in the Center for Cancer Research Sequencing Facility at the National Institutes of Health (Bethesda, MD). Reads of the samples were trimmed for adapters and low-quality bases using Trimmomatic software before alignment with the reference genome mouse-mm10 and annotated transcripts using STAR. Gene counts were filtered by genes with $\geq$5 reads and normalized to the trimmed mean of M values using Partek Flow software, version 8 (Partek, Chesterfield, MO). Trimmed Mean of M values normalized counts was used for differential analysis using PARTEK Flow GSA algorithm (Partek). Gene Ontology terms were obtained with ToppGene (Chen et al., 2009) using

indicated gene sets. Canonical pathways and upstream regulators analysis were generated with Ingenuity Pathway Analysis (Ingenuity Systems, www.ingenuity.com) using genes with $q < 0.05$ and fold change (FC) ≥ 2.0. Analysis of over-represented conserved transcription factor binding sites was performed with oPOSSUM (Kwon et al., 2012) using upregulated ($q < 0.05$, FC ≥ 2.0) and downregulated ($q < 0.05$, FC ≤ -2.0) genes, looking at 2 kilobase upstream/downstream sequence with a conservation cutoff of 0.6. Differentiation gene clusters and functional signature genes for cell adhesion and extracellular matrix were obtained from Joost et al. (2016). SNAI2-overexpressing gene expression profile in the keratinocytes was extracted from GSE55269. The microarray data were processed through R, and the differently expressed genes were calculated by Limma package. Upstream regulators analyses were generated with Ingenuity Pathway Analysis (Ingenuity Systems, www.ingenuity.com) using genes with $q < 0.05$ and FC ≥ 2.0. Genes downregulated both by SNAI2 and KLF4 by pooled-small interfering RNAs were sent to Gene Ontology terms enrichment analysis with ToppGene. Gene set enrichment analysis preranked enrichment analysis was conducted through the gene set enrichment analysis 4.1.0 client with the default setting. Genes with YAP1-binding sites were ranked on the basis of the $\log_2$ FC and were matched to the gene set enrichment analysis gene signature datasets c5.go.bp.v7.4.symbols.

Chromatin immunoprecipitation sequencing and CUT&RUN qPCR

For chromatin immunoprecipitation (ChIP) sequencing experiments, cells were fixed with 1% formaldehyde for 15 minutes and quenched with 0.125 M glycine and sent to Active Motif Services (Carlsbad, CA) to be processed for ChIP sequencing. In brief, chromatin was isolated by the addition of lysis buffer, followed by disruption with a Dounce homogenizer. Lysates were sonicated, and the DNA was sheared to an average length of 300−500 base pairs. Genomic DNA (Input) was prepared by treating aliquots of chromatin with RNase, proteinase K, and heat for decross linking, followed by ethanol precipitation. Pellets were resuspended, and the resulting DNA was quantified on a NanoDrop spectrophotometer (Thermo Fisher Scientific, Waltham, MA). Extrapolation to the original chromatin vol-ume allowed quantitation of the total chromatin yield. An aliquot of chromatin (30 µg) was precleared with protein A agarose beads (Invitrogen). Genomic DNA regions of interest were isolated using 4 µg of antibody against YAP1 (United States Biological, Salem, MA, catalog #Y1200-01D). Com-plexes were washed, eluted from beads with SDS buffer, and subjected to RNase and proteinase K treatment. Crosslinks were reversed by incubation overnight at 65 °C, and ChIP DNA was purified by phenol–chloroform extraction and ethanol precipitation. Illumina sequencing libraries were prepared from the ChIP and Input DNAs by the standard consecutive enzymatic steps of end polishing, dA-addition, and adaptor ligation. Steps were performed on an auto-mated system (Apollo 342, WaferGen Biosystems/Takara Bio, Shiga, Japan). After a final PCR amplification step, the resulting DNA libraries were quantified and sequenced on Illumina's NextSeq 500 (75 nucleotides reads, single end). Reads were aligned to the human genome (hg38) using the BWA algorithm (default settings). Duplicate reads were removed, and only the uniquely mapped reads (mapping quality ≥25) were used for further analysis. Alignments were extended in silico at their 3′-ends to a length of 200 base pairs, which is the average genomic fragment length in the size-selected library, and assigned to 32-nucleotides bins along the genome. The resulting histograms (genomic signal maps) were stored in bigWig files. Peak locations were determined using the MACS algorithm (version 2.1.0) with a cutoff of $P = 1e\text{-}5$. Peaks that were on the ENCODE blacklist of known false ChIP-sequencing peaks were removed. HOMER motif enrichment analysis was conducted with HOMER software. ChIP CUT&RUN qPCR was performed with Cell Signaling CUT&RUN Assay Kit (Cell Signaling Technology, Danvers, MA, #86652) according to the manufacturer's instructions. Briefly, cells infected with adenoviruses expressing GFP or adenoviruses expressing a GFP-tagged TEAD inhibitor were collected at room temperature and counted, and 2 × 10e5 cells were used for each reaction. qPCR reactions were carried out in triplicate on specific genomic regions using Applied Biosystem Power SYBR Green PCR Master Mix (catalog number 4367659). The resulting signals were normalized for primer efficiency by carrying out qPCR for each primer pair using Input DNA. Antibody against YAP1 (Cell Signaling Technology; clone number D8H1X; catalog number 14074; 1:50) was used at 1:50 dilution. Primers used were *CCN2* forward TGAGTTGATGAGGCAGGAAGG and *CCN2* reverse CACAAACAGGGACATTCCTCG, *SNAI2* primer1 forward TTGGCTTTTTGGAGGCGTTG and *SNAI2* primer1 reverse GATGCTGTAGGGACCGCC, and *SNAI2* primer2 forward CGAGTAACACGTATGCCCGT and *SNAI2* primer2 reverse TTCGTCTGACTCACGCCATC. KLF4 ChIP-sequencing data were from Szigety et al. (2020). KLF4 function prediction was performed by BETA (Binding and expression target analysis) 1.0.7 (Wang et al., 2013), following the basic instructions. Predicted direct KLF4 target genes were sent to Gene Ontology terms enrichment analysis with ToppGene.

Mice

All mouse studies were carried out according to approved protocols from the National Institute of Health Intramural Animal Care and Use Committee of the National Cancer Institute (Bethesda, MD), in compliance with the Guide for the Care and Use of Laboratory Animals. Tetracycline-inducible TEAD inhibitor (TRE-TEADi) mice were described before (Yuan et al., 2020). Other mouse lines were obtained from the Jackson Laboratory (Bar Harbor, ME): LSL-SmoM2 (stock 005130), LSL-rtTA (stock 005670), and K14CreERT (stock 005107). Both LSL-SmoM2 and LSL-rtTA transgenes are in the same Rosa26 locus. To generate K14CreERT$^{+/-}$ LSLSmoM2$^{+/-}$ LSL-rtTA$^{+/-}$ TRE-TEADi$^{+/-}$ mice, homozygous K14-SmoM2 mice were crossed with LSL-rtTA homozygous-TRE-TEADi heterozygous mice. Both male and female mice were used, and all experiments were conducted using littermate controls. Housing conditions were as follow: temperature set point was 72 ± 4 °F (22.2 ± 2.2 °C), light cycle of 12 hours on 6 AM to 6 PM and 12 hours off, and National

Institute of Health-03I rodent diet. Tamoxifen (Sigma-Aldrich) was dissolved in ethanol and mixed in oil (Miglyol 810N, Peter Cremer North America LP, Cincinnati, OH) for intraperitoneal injection in mice at a dose of 100 mg/kg. Doxycycline was administered in food grain–based pellets (Bio-Serv, Flemington, NJ) at 6 g/kg.

Immunofluorescence and immunohistochemistry

Immunofluorescence analysis of mouse skin was performed on tissue sections embedded in paraffin. Sections were rehydrated and prepared for staining by antigen retrieval in 10 mM sodium citrate buffer (pH 6), washed, and blocked with 3% BSA for 1 hour at room temperature. Slides were incubated with the primary antibody overnight at 4 °C and washed three times with PBS followed by incubation with the secondary antibody for 1.5 hours at room temperature. Sections were mounted in FluorSave Reagent (Millipore, Burlington, MA, #345789) with #1.5 coverslips for imaging. Nuclei were stained with Hoechst 33342 (1:2,000, Invitrogen, #H3570). The following antibodies were used: GFP (Aves Labs, Tigard, OR; catalog number GFP-1010; 1:500), K10 (BioLegend, San Diego, CA; catalog number 905401; 1:400), proliferating cell nuclear antigen (Cell Signaling Technology; catalog number 13110S; 1:400), p63 (Cell Signaling Technology; catalog number 39692S; 1:400), mouse KLF4 (R&D Systems; catalog number AF3158; 1:200, 5 μg/ml), and K14 (BioLegend; catalog number 906001; 1:400). The secondary antibodies were Donkey anti-Rabbit IgG Alexa Fluor 555 (Invitrogen; catalog number A-31572; 1:1,000), Donkey anti-Goat IgG Alexa Fluor 546 (Invitrogen; catalog number A-11056; 1:1,000), and Goat anti-Chicken IgY Alexa Fluor 488 (Invitrogen; catalog number A-11039; 1:1,000). Images were obtained using a Keyence BZ-X700 with automatic stage and focus with BZX software (Nikon objectives CFI Plan Apo λ20 × numerical aperture 0.75 and CFI Plan Apo λ10 × numerical aperture 0.45, Nikon, Tokyo, Japan). Final images were bright contrast adjusted with BZX analysis software (Keyence, Osaka, Japan). For quantification, images were obtained with a ×10 objective with the same exposure condition for each antibody target staining. Quantification was done in the BZX analysis software (Keyence) equipped with hybrid cell count and macrocell count. The GFP-positive and -negative cells were analyzed separately through individual channels. Multiple fields per mouse were analyzed at the same counting conditions by the software automatically. For histological analysis, tissues were embedded in paraffin, and 3-μm sections were stained with H&E. Stained H&E slides were scanned at ×40 using an Aperio CS Scanscope (Leica Microsystems, Wetzlar, Germany). Tumor burden level was quantified in the ear H&E sections by HALO image analyzing platform provided by the National Institutes of Health. By training a random forest learning model, the HALO image classifier model can classify the whole BCC epidermis and produce a confidence probability mask. Areas with a probability >50% were analyzed, and areas <200 μm were excluded. For each mouse, the ear was trimmed vertically, and 4–6 different trimming sections were quantified, and the average area of these sections was considered as the mouse tumor burden level. Sections across an ear tag site were excluded when annotating the quantification layers. Immunohistochemistry staining of mouse skin was performed on tissue sections embedded in paraffin. Sections were prepared for staining by antigen retrieval in 10 mM sodium citrate buffer (pH 6), washed, and blocked with 3% BSA for 1 hour at room temperature. Slides were then incubated with primary antibody YAP1 (Cell Signaling Technology; clone number D8H1X; catalog number 14074; 1:100) and GLI1 (R&D System, AF3455, 1:100, 1 μg/ml) overnight at 4 °C and were washed three times with PBS. Secondary antibody incubation and horseradish peroxidase reaction were conducted with Vectastain ABC kit horseradish peroxidase (Vector Laboratories, Burlingame, CA).

Immunoblot analysis

For western blot, cells were lysed by sonication at 4 °C in lysis buffer (50 mM Tris-hydrochloric acid, 150 mM sodium chloride, 1 mM EDTA, 1% Nonidet P-40, 0.5% sodium deoxycholate, 0.1% SDS) supplemented with complete protease inhibitor cocktail (Roche, Basel, Switzerland, #6538304001) and phosphatase inhibitors (PhosSTOP, Sigma-Aldrich, #4906837001). Equal amounts of total cell lysate proteins were subjected to SDS-PAGE and transferred to polyvinylidene difluoride membranes. Primary antibodies used were anti-GAPDH (Cell Signaling Technology; clone number 14C10; catalog number 2118; 1:2,000), anti-GFP (Cell Signaling Technology; clone number D5.1; catalog number 2956; 1:2,000), K10 (BioLegend; catalog number 905401; 1:1,000), STAT3 (Cell Signaling Technology; clone number D1B2J; catalog number 30835; 1:1,000), phosphorylated STAT3 (Tyr705) (Cell Signaling Technology; clone number D3A7; catalog number 9145; 1:1,000), KLF4 (R&D Systems; catalog number AF3158; 1:1,000, 1 μg/ml), YAP1 (Cell Signaling Technology; clone number D8H1X; catalog number 14074; 1:1,000), TAZ (Cell Signaling Technology; clone number V386; catalog number 4883; 1:1,000), and SNAI2 (Cell Signaling Technology; clone number C19G7; catalog number 9585; 1:1,000). Secondary horseradish peroxidase–conjugated antibodies used were Pierce peroxidase goat anti-mouse IGG (H+L) (Thermo Fisher Scientific, catalog number 31432; 1:4,000) and Pierce peroxidase goat anti-rabbit IGG (H+L) (Thermo Fisher Scientific; catalog number 31462; 1:4,000). The secondary antibody was incubated at room temperature for 1 hour. Bands were detected using a ChemiDoc Imaging System (Bio-Rad Laboratories, Hercules, CA) with Clarity Western ECL Blotting Substrates (Bio-Rad Laboratories) according to the manufacturer's instructions. Blot images were processed using ImageLab software, version 5.2.1 (Bio-Rad Laboratories).

SUPPLEMENTARY REFERENCES

AlAmri MA, Kadri H, Alderwick LJ, Jeeves M, Mehellou Y. The photosensitising clinical agent verteporfin is an inhibitor of SPAK and OSR1 kinases. ChemBioChem 2018;19:2072–80.

Chen J, Bardes EE, Aronow BJ, Jegga AG. ToppGene Suite for gene list enrichment analysis and candidate gene prioritization. Nucleic Acids Res 2009;37(Web Server Issue):W305–11.

de Thé H. Differentiation therapy revisited. Nat Rev Cancer 2018;18:117–27.

Iglesias-Bartolome R, Torres D, Marone R, Feng X, Martin D, Simaan M, et al.

Inactivation of a Gα(s)-PKA tumour suppressor pathway in skin stem cells initiates basal-cell carcinogenesis. Nat Cell Biol 2015;17:793−803.

Jiao S, Wang H, Shi Z, Dong A, Zhang W, Song X, et al. A peptide mimicking VGLL4 function acts as a YAP antagonist therapy against gastric cancer. Cancer Cell 2014;25:166−80.

Joost S, Zeisel A, Jacob T, Sun XY, La Manno G, Lönnerberg P, et al. Single-cell transcriptomics reveals that differentiation and spatial signatures shape epidermal and hair follicle heterogeneity. Cell Syst 2016;3:221−37.e9.

Kim M, Kim M, Lee S, Kuninaka S, Saya H, Lee H, et al. cAMP/PKA signalling reinforces the LATS-YAP pathway to fully suppress YAP in response to actin cytoskeletal changes. EMBO J 2013;32:1543−55.

Kwon AT, Arenillas DJ, Worsley Hunt R, Wasserman WW. oPOSSUM-3: advanced analysis of regulatory motif over-representation across genes or ChIP-seq datasets. G3 (Bethesda) 2012;2:987−1002.

Li Z, Zhao B, Wang P, Chen F, Dong Z, Yang H, et al. Structural insights into the YAP and TEAD complex. Genes Dev 2010;24:235−40.

Liu-Chittenden Y, Huang B, Shim JS, Chen Q, Lee SJ, Anders RA, et al. Genetic and pharmacological disruption of the TEAD-YAP complex suppresses the oncogenic activity of YAP. Genes Dev 2012;26:1300−5.

Makinodan E, Marneros AG. Protein kinase A activation inhibits oncogenic Sonic hedgehog signalling and suppresses basal cell carcinoma of the skin. Exp Dermatol 2012;21:847−52.

McNeill H, Woodgett JR. When pathways collide: collaboration and connivance among signalling proteins in development. Nat Rev Mol Cell Biol 2010;11:404−13.

Piccolo S, Dupont S, Cordenonsi M. The biology of YAP/TAZ: hippo signaling and beyond. Physiol Rev 2014;94:1287−312.

Scott LJ, Goa KL. Verteporfin. Drugs Aging 2000;16:139−46. discussion 47−8.

Szigety KM, Liu F, Yuan CY, Moran DJ, Horrell J, Gochnauer HR, et al. HDAC3 ensures stepwise epidermal stratification via NCoR/SMRT-reliant mechanisms independent of its histone deacetylase activity. Genes Dev 2020;34:973−88.

Wang S, Sun H, Ma J, Zang C, Wang C, Wang J, et al. Target analysis by integration of transcriptome and ChIP-seq data with BETA. Nat Protoc 2013;8:2502−15.

Yu FX, Zhang Y, Park HW, Jewell JL, Chen Q, Deng Y, et al. Protein kinase A activates the Hippo pathway to modulate cell proliferation and differentiation. Genes Dev 2013;27:1223−32.

Yuan Y, Park J, Feng A, Awasthi P, Wang Z, Chen Q, et al. YAP1/TAZ-TEAD transcriptional networks maintain skin homeostasis by regulating cell proliferation and limiting KLF4 activity. Nat Commun 2020;11:1472.

Zhang Z, Lin Z, Zhou Z, Shen HC, Yan SF, Mayweg AV, et al. Structure-based design and synthesis of potent cyclic peptides inhibiting the YAP-TEAD protein-protein interaction. ACS Med Chem Lett 2014;5:993−8.

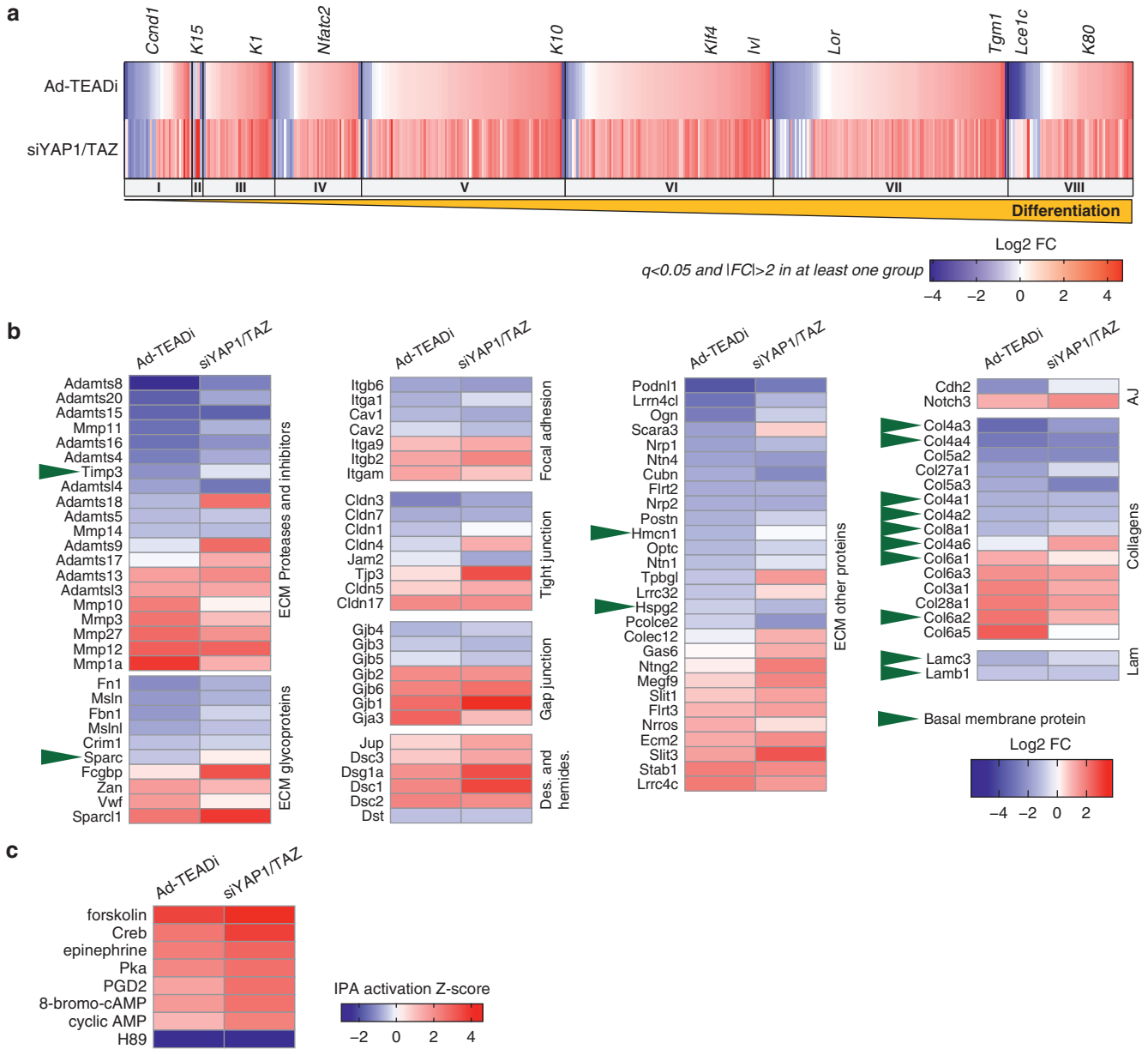

Supplementary Figure S1. Effects of TEAD inhibition in BCC cells. (**a**) Heatmap showing FC of differentiation markers in TEADi and siYAP1/TAZ datasets ($q < 0.05$ and $FC \geq 2$ in at least one condition); clusters of differentiation genes from basal (I) to terminal differentiation (VIII) and key differentiation markers are indicated. (**b**) Expression changes in ECM and cell adhesion components in TEADi and siYAP1/TAZ datasets ($q < 0.05$ and $FC \geq 2$ in at least one condition). Basal membrane proteins are highlighted by arrows. (**c**) Heatmap showing the activation Z-score for selected IPA upstream transcriptional regulators related to cAMP and PKA signaling in genes differentially regulated in siYAP1/TAZ or TEADi datasets ($q < 0.05$ and $FC \geq 2$). Forskolin, epinephrine, and PGD2 are activators of cAMP and PKA. H89 is an inhibitor of the kinase activity of PKA. Ad-TEADi, adenoviruses expressing a GFP-tagged TEAD inhibitor; BCC, basal cell carcinoma; ECM, extracellular matrix; FC, fold change; IPA, ingenuity pathway analysis; K, keratin; PKA, protein kinase A; siYAP1/TAZ, small interfering RNAs targeting YAP1 and TAZ; TEADi, TEAD inhibitor.

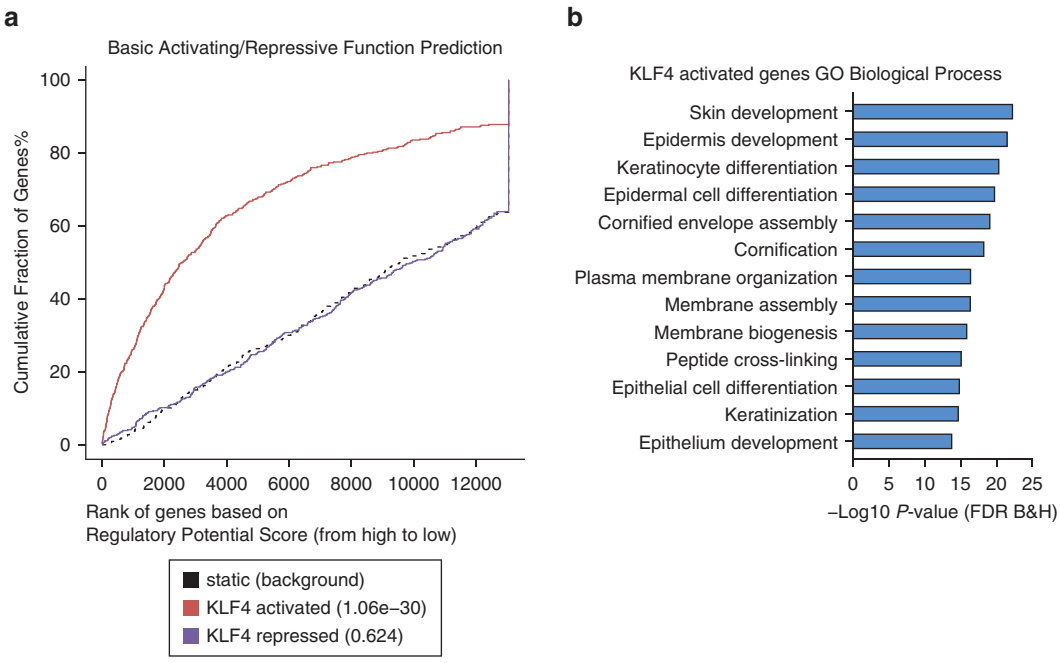

Supplementary Figure S2. Prediction of KLF4 activity in TEADi BCC cells. (**a**) BETA indicating the predicted activation of KLF4 in TEADi BCC cells. (**b**) Graph shows the top GO terms enriched in predicted KLF4-activated genes in TEADi BCC cells. BCC, basal cell carcinoma; BETA, binding and expression target analysis; FDR, false discovery rate; GO, gene ontology; TEADi, TEAD inhibitor.

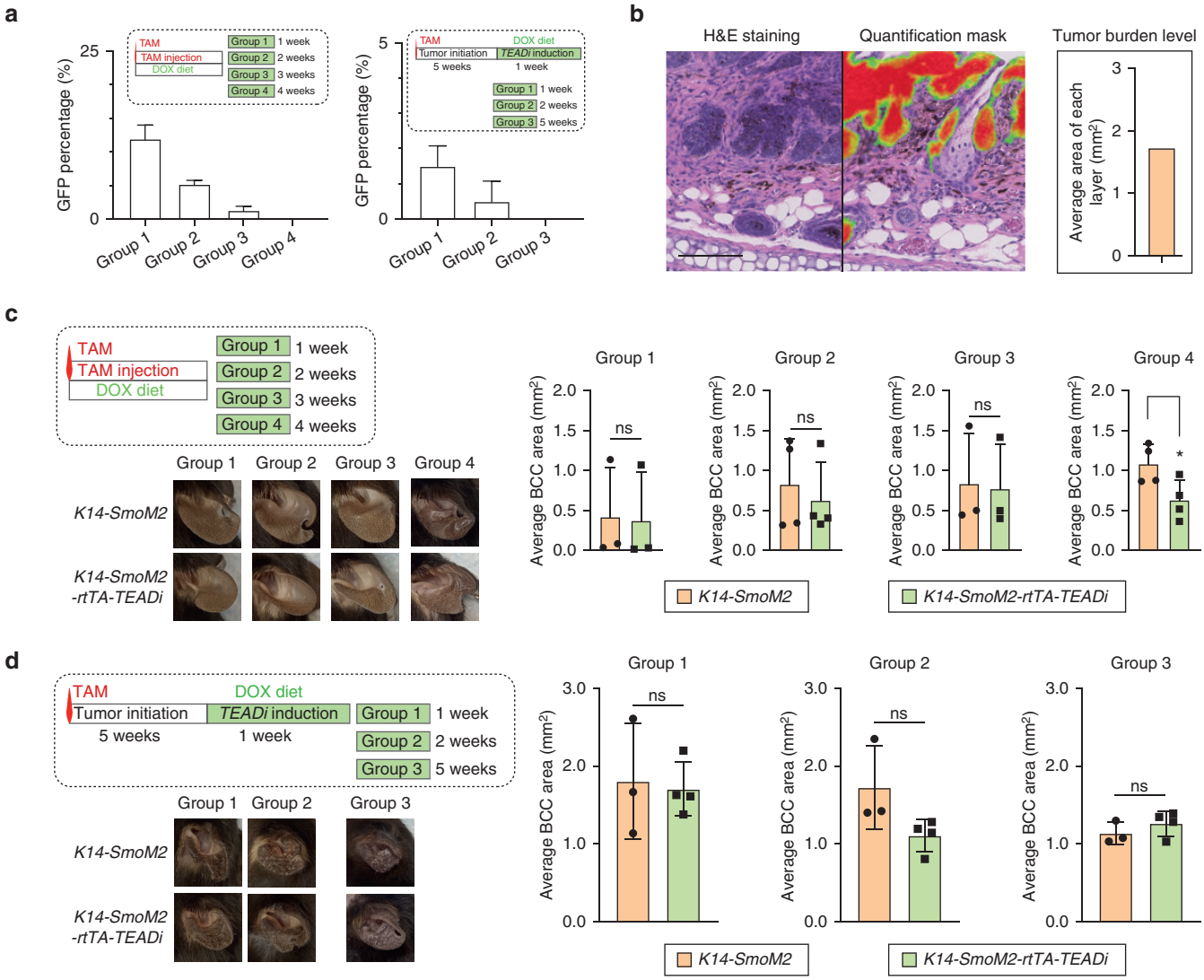

Supplementary Figure S3. Quantification of tumor burden in BCC. (**a**) Quantification of the percentage of GFP-positive cells in the ear of BCC mouse model in the indicated groups. (**b**) HALO quantification workflow and mask showing the BCC ear area identified by the software; tumor burden level represented the average area of the different trimming sections (Bar = 100 μm). (**c, d**) Timeline, representative pictures, and quantification of ear epidermis tumor burden in mice induced to form BCC tumors concomitantly expressing or not expressing TEADi. Each dot represents an individual mouse for the quantification; for **c**, n = 3 mice for groups 1 and 3 and n = 4 mice for groups 2 and 4; for **d**, n = 4 mice analyzed for groups 1–3; two-tailed unpaired *t*-test (*$P < 0.05$). Ear pictures are from different mice harvested at the indicated time points. BCC, basal cell carcinoma; DOX, doxycycline; K14, keratin 14; ns, nonsignificant; TAM, tamoxifen; TEADi, TEAD inhibitor.